Ionics (2022) 28:4685–4695
https://doi.org/10.1007/s11581-022-04707-z

ORIGINAL PAPER

Facile synthesis of N, S co-doped $CoMoO_4$ nanosheets as high-efficiency electrocatalysts for hydrogen evolution reaction

Jie Wang[1] · Haicheng Xuan[1] · Lingxin Meng[1] · Jiangtao Yang[1] · Jiale Yang[1] · Xiaohong Liang[1] · Yuping Li[1] · Peide Han[1]

Received: 4 July 2022 / Revised: 26 July 2022 / Accepted: 27 July 2022 / Published online: 10 August 2022

Abstract

The development of low-cost and high-efficiency hydrogen evolution reaction (HER) electrocatalysts has become extremely essential to address global energy issues. Herein, we have fabricated arrays of nitrogen and sulfur co-doped $CoMoO_4$ ultrathin nanosheets grown on nickel foam (N, S-$CoMoO_4$/NF_{400}). The experimental results demonstrate that modulating the electronic structure of $CoMoO_4$ by co-doping N and S atoms is one of the most powerful methods to boost the performance of HER. N, S-$CoMoO_4$/NF_{400} displays superior HER activity under alkaline environment, with overpotentials of 58 and 119 mV at 10 and 100 mA cm^{-2}. The excellent performance of the N, S-$CoMoO_4$/NF_{400} electrode proves that the N, S co-doping engineering can significantly improve the catalytic activity of transition metal-based oxide HER.

Keywords Hydrogen evolution reaction · Nanosheet arrays · N · S co-doped · Electrocatalysis

Introduction

The massive consumption of fossil fuels has led to a global energy crisis, and it is vital to develop green and sustainable utilization of energy [1]. As a clean, non-polluting, renewable energy with high energy density by weight, hydrogen exhibits broad application prospects in energy conversion and energy storage system [2, 3]. Among the various scalable methods for high-purity hydrogen production, electrocracking of water is one of the most convenient and environment friendly strategies [4, 5]. Currently, the precious metal platinum is the most active electrocatalyst for catalytic hydrogen evolution reactions, but its scarcity and instability have prevented its widespread application [6, 7]. For this reason, it is imperative to develop earth-rich and non-noble metal catalysts to replace Pt-based electrocatalysts.

In recent years, a wide spectrum of transition-metal oxides [8, 9], sulfides [10, 11], and phosphides [12, 13], have exhibited excellent catalytic performance for HER. Among the many non-precious metal electrocatalysts, transition metal oxide (TMOs) catalysts are of great interest owing to their low price, abundant reserves, low toxicity and high activity [14, 15]. Various modification methods have been used to solve the above problems, such as doping engineering, vacancy engineering, and morphology control [16]. Currently, bimetallic cobalt-molybdenum oxide ($CoMoO_4$) is of great interest due to the fact that the composite of two elements of CoMo can be an efficient electrocatalytic material [17–20]. However, with the limited electrochemical active sites and low electrical conductivity, pure $CoMoO_4$ still maintains undesirable HER performance, which is an urgent problem to be solved [21]. Among the above modification methods, doping engineering with non-metallic elements is widely used. The reason is that with a large variety of available doping elements, the electrochemical properties of transition metal oxides can be optimized from multiple aspects [22]. For example, the doping of N atoms can enhance the HER performance of the catalyst dramatically. The small radius of N atoms has a tendency to occupy the gaps between metal atoms forming a dense lattice interstitial structure which is close to that of pure metal catalysts, resulting in strong metal abundance and fast electron transfer rates [23]. Recently, Xie et al. revealed that the doping of nitrogen could change the surface properties of $CoMoO_4$, and the high-valent Mo ions were reduced to the low-valent state, which enhanced the HER performance [17]. Huang and co-workers fabricated N-doped Ni-Mo-based sulfides with the nickel foam substrates, showing low overpotential values of 68 and 322 mV at HER current densities of 10 and

✉ Haicheng Xuan
xuanhaicheng@tyut.edu.cn

[1] College of Materials Science and Engineering, Taiyuan University of Technology, Taiyuan 030024, People's Republic of China

1000 mA cm^{-2}. Experimental results show that the entry of N atoms into the substrate lattice reduces H atoms adsorption energy of the catalysts and modulates the electron density of the sulfides, which enhances the electronic conductivity and accelerates the HER process [24]. Moreover, the doping of S atoms is also reported to be a feasible method for enhancing the catalytic performance of the composites. The doping of S atoms could increase the oxygen vacancies and induce defects on the catalyst substrate surface, which is beneficial to boost the HER activity [25]. Sun et al. found that the doping of S elements could cause epitaxial phase transition and surface reconfiguration of the catalyst, increasing the cation redox centers [26]. Wang and associates reported that the type and number of $VMoO_x$ active centers were improved by S doping and induced a reasonably effective synergistic effect, which presented a overpotential of 73 mV for HER at 10 mA cm^{-2} [27]. Actually, the majority of the current studies have focused on the single element N or S doping of composites. Recently, Naveen et al. prepared a N, S co-doped coordination polymer with an operating potential of only 30 mV at a current density of 10 mA cm^{-2} [28]. Experiments reveal that the HER performance of electrode materials can be effectively enhanced by the co-doping of N and S atoms. Combined with the above discussion, it is proved that the N and S co-doping can be more effective to modulate the electron density of metal nanoparticles and change the electronic structure of the particles, which is promising to further enhance the HER performance of the electrode.

In this work, we propose to prepare $CoMoO_4$ precursors by a simple hydrothermal method, and then fabricate N, S co-doped $CoMoO_4$ nanosheet arrays with atmosphere treatment strategy. The results reveal an effective enhancement of the electrical conductivity of the nanosheets via N, S co-doping, an optimization of the Co/Mo-H* interaction and a significant reduction of the energy barrier to water dissociation. Based on the beneficial composition and outstanding structural advantages, the formed N, S-$CoMoO_4$/NF_{400} nanosheet arrays exhibit excellent HER activity. The catalysts have low overpotentials of 58 and 119 mV at current densities of 10 mA cm^{-2} and 100 mA cm^{-2}. This work provides an economical and efficient HER catalyst that improves the electrocatalytic performance of transition metal-based electrocatalysts, and also demonstrates an effective strategy for designing efficient water cracking catalysts.

Experimental section

Materials

The nickel foam (NF) was produced by Changde Liyuan New Material Co., Ltd. Cobaltous nitrate hexahydrate ($Co(NO_3)_2{\cdot}6H_2O$), and Sodium molybdate (vi) dihydrate ($Na_2MoO_4{\cdot}2H_2O$) were supplied by Shanghai Aladdin Biochemical Technology Co., Ltd. Urea (CH_4N_2O), Sulfur sublimed (S), ethanol (C_2H_5OH), acetone (CH_3CHO) and hydrochloric acid (HCl) were also used for experiments.

Synthesis of $CoMoO_4$/NF

In a typical synthesis, 1.25 mmol of $Na_2MoO_4{\cdot}2H_2O$ and $Co(NO_3)_2{\cdot}6H_2O$ (Co:Mo = 1:1) were added to 40 mL of deionized water. The solution was stirred uniformly and transferred to a 50 mL Teflon-lined stainless-steel autoclave. After holding at 180 °C for 12 h, the NF was removed and washed several times with distilled water, and then dried at 60 °C for 12 h. Finally, the hydrothermal prepared NF was annealed in air at 500 °C for 2 h.

Synthesis of N, S-$CoMoO_4$/NF_x

N, S-$CoMoO_4$/NF_x were prepared via chemical vapor deposition (CVD) at 300℃, 400℃, and 500℃ for 2 h in N_2 atmosphere, where sulfur powder and urea were the sources of S and N elements. The obtained working electrodes were named as N, S-$CoMoO_4$/NF_{300}, N, S-$CoMoO_4$/NF_{400}, N, S-$CoMoO_4$/NF_{500}, respectively. As a comparison, S-$CoMoO_4$/NF and N-$CoMoO_4$/NF nanosheet arrays were obtained by the same method, except that sulfur and urea were added separately at 400℃.

Synthesis of Pt/C catalyst on NF

To make Pt/C/NF catalyst, commercial catalyst (5 mg) was dispersed in a mixture of 180 ml of isopropyl alcohol and 20 ml of 5% Nafion to form a homogeneous ink. The catalyst ink was dropped on NF (1 cm × 1 cm) with a catalyst loading of 2 mg.

Characterizations

The crystallinity of the sample was calibrated by X-ray diffraction (XRD, Bruker D8 Advance, scanning range 10–80°, scanning speed 2°/min). Scanning electron microscopy (SEM, Hitachi, S2400) and transmission electron microscopy (TEM, FEI Talos F200S) were applied to study the microstructure of all samples. Elemental species, compositions and valence states were obtained by X-ray photoelectron spectroscopy (XPS) of the PHI Quantera II electron spectrometer.

Electrochemical measurements

Electrochemical tests were conducted by CHI660e electrochemical workstation. The Hg/HgO electrode and the Pt electrode were chosen as the reference electrode and counter

electrode, respectively. The 1 M KOH solution (PH = 13.8) was used as the electrolyte. Linear sweep voltammetry (LSV) was used to evaluate the working electrode activity at a scan rate of 2 mV s^{-1}. Cyclic voltammetry (CV) curves were used to measure the capacitance values of the bilayer at scan rates of 5 to 25 mV s^{-1}. Electrochemical impedance spectroscopy (EIS) was tested in the range between 0.1 Hz and 10^5 Hz. All potentials were converted to RHE by Nernst equation ($E_{RHE} = E_{Hg/HgO} + 0.0591pH + 0.098$).

Result and discussion

Figure 1 depicts the procedure for the preparation of N, S-$CoMoO_4/NF_x$. Firstly, this work successfully synthesized $CoMoO_4$/NF nanosheet arrays on NF substrates with a hydrothermal method. The formation of N, S-$CoMoO_4/NF_x$ can be reflected by the change of the surface color in the electrocatalysts. Clearly, the bare NF turns lavender after the hydrothermal reaction, then becomes dark yellow during the annealing and finally changes into black after the N, S doping process. The changes in color indicate that the phase composition of the catalyst has been transformed through atmospheric treatment.

Figure 2a-c shows the SEM images of the CoMo-precursors from high magnification to low magnification. After hydrothermal treatment, the precursors show a smooth sheet-like structure with a lateral size of about 1.4 μm. Low magnification image shows the formation of the flower cluster structure due to the accumulation of nanosheets, providing a mass of nucleation sites. Figure 2d-f shows SEM images of the $CoMoO_4$ nanosheet arrays at different resolutions after high temperature calcination. The lateral size decreases after high temperature annealing at 500 °C. $CoMoO_4$/NF possesses a rough surface and the clusters are more closely packed than before. Figure 2g-i are SEM images of N, S-$CoMoO_4/NF_{400}$. Notably, the structure of nanosheet arrays is well maintained after N, S co-doping of the catalysts, and the N, S-$CoMoO_4/NF_{400}$ nanosheets grown on nickel foam are further reduced. The above results clearly show that the NF is loaded with a large number of nanosheets and the ultrathin nanosheets are grown uniformly. These ultra-thin nanosheets would provide more active sites for HER processes and enhance their close contact with the electrolyte, increasing the mass transfer efficiency. Moreover, the catalysts morphology is significantly affected by the heat treatment temperature, which is also experimentally investigated. Figs. S1 and S2 show SEM images of N, S-$CoMoO_4/NF_{300}$ and N, S-$CoMoO_4/NF_{500}$. At relatively low heat treatment temperatures, the reduction in the number of nanosheets grown on NF results in a lower number of exposed active sites. When the temperature is raised to 500 °C, the nanosheets are transformed into needles. The needle-like structure is sparsely distributed and reduces the mass transfer rate, resulting in low electrochemical activity. SEM images of the pure nitride and pure sulfide doping samples are also investigated, as shown in Figs. S3 and S4, revealing the rough surface. The above morphological comparison shows that N, S-$CoMoO_4/NF_{400}$ benefits from a porous ultra-thin sheet structure that can expose abundant active sites. The ultra-thin nanosheet arrays have a large specific surface area, which can enable close contact at the

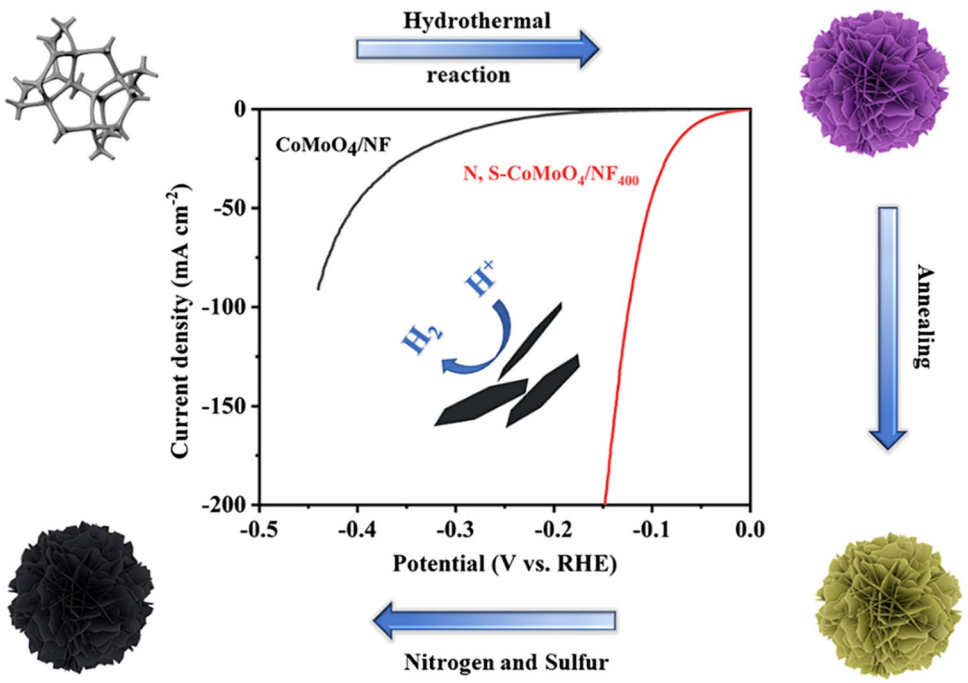

Fig. 1 Schematic diagram of the preparation of N, S-CoMoO4/NF400 nanosheet arrays

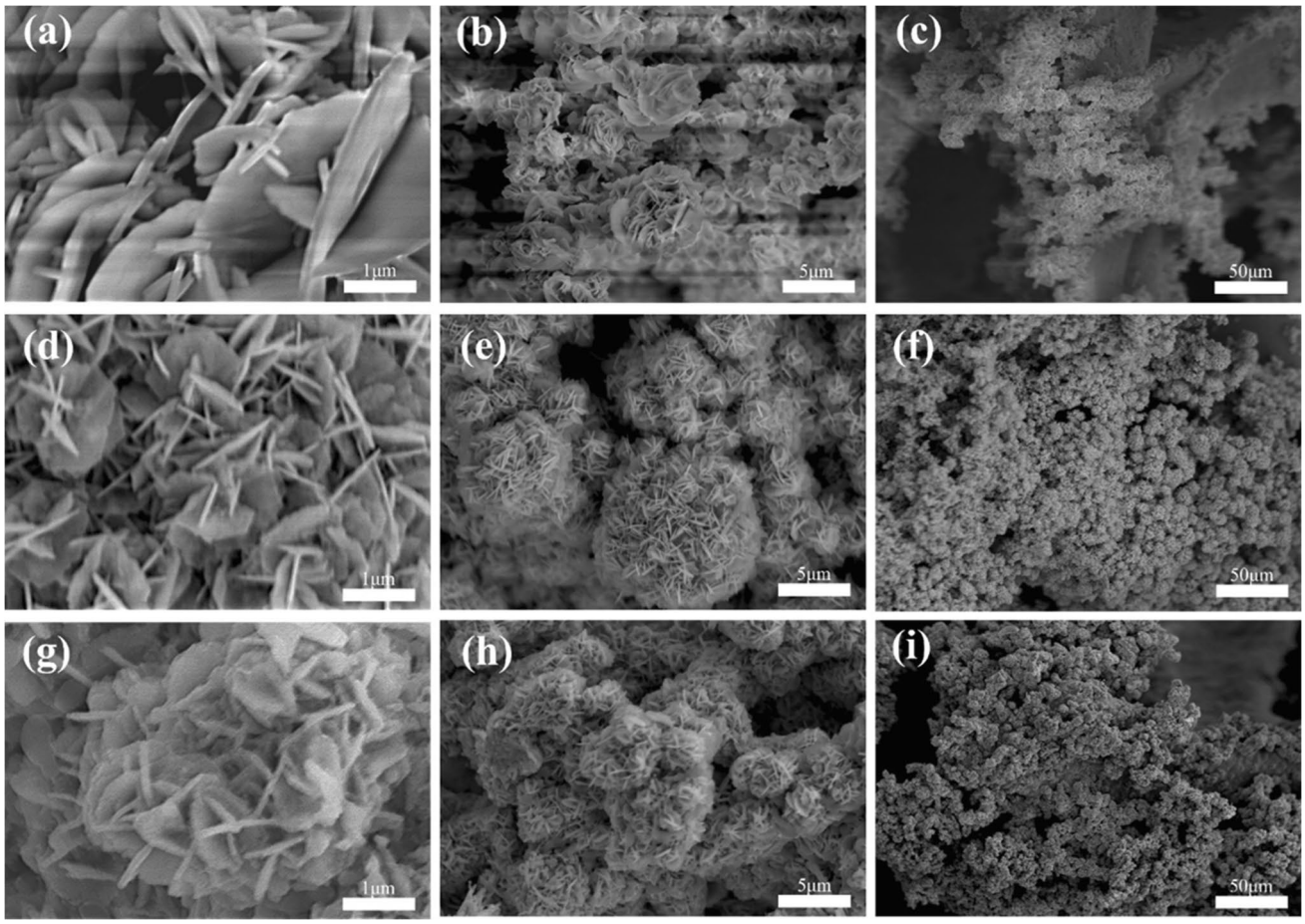

Fig. 2 SEM images of (**a**–**c**) CoMo precursors, (**d**–**f**) CoMoO4 and (**g**–**i**) N, S-CoMoO4/NF400

electrode/electrolyte interface, accelerate the gas release rate, and facilitate the structural stability of the catalyst during operation.

XRD was employed to evaluate the chemical composition of all samples. N, S-$CoMoO_4/NF_{400}$ displays three strong characteristic peaks at 44.45°, 51.86° and 76.37°, which is in good correspondence with Ni (PDF#04–0850) (Fig. 3) [29]. Other characteristic peaks demonstrate that the N, S-$CoMoO_4/NF_{400}$ is hybrid of $CoMoO_4$ (PDF#21–0868) [30], CoS_2 (PDF#41–1471) [31], and MoS_2 (PDF#02–1133) [24]. After N, S co-doping, the characteristic peak at 25.51° of the (002) plane of $CoMoO_4$ is slightly shifted to a higher diffraction angle, which can be due to the reduction of the crystal plane spacing as a result of the N atom occupying the O sites. Similarly, Fig. 2 also shows that the characteristic peaks at 62.7° and 33.21° attributed to the (102) plane of CoS_2 and the (100) plane of MoS_2, respectively, are shifted toward higher diffraction angles. This is caused by the substitution of S atoms by N atoms with smaller radius [32]. The above results demonstrate that N and S have been successfully doped into the crystals of $CoMoO_4$. Fig. S5a and b shows the phase compositions of the samples obtained at the atmosphere temperatures of 300 °C and 500 °C. Low-temperature sulfidation produces Co_3S_4 and Mo_3S_4 phases. The stability and conductivity of the Co_3S_4 phase are lower than those of the CoS_2 phase, respectively [32]. Although the HER activity of the Mo_3S_4 phase is comparable to that of the MoS_2 phase, the cathodic desorption of $[Mo_3S_4]^{4+}$ from the catalyst support is gradually slow with time [33]. When the temperature is increased, the sulfur powder reacts with the nickel foam substrate to form the NiS_2 phase. The N doping greatly reduces the hydrogen adsorption free energy (ΔG_{*H}) of NiS_2 [24]. Fig. S5c and d shows the XRD images of N-$CoMoO_4$/NF and S-$CoMoO_4$/NF. The presence of nitride and sulfide phases reveals the successful doping of N and S atoms into the compounds. The above results show that the CoS_2 and MoS_2 phases with higher conductivity are produced by annealing at 400 °C. Meanwhile, the doping of nitrogen and sulfur can effectively reduce the ΔG_{*H} of Co and Mo, which is beneficial for the electrocatalyst to improve the HER performance [34, 35].

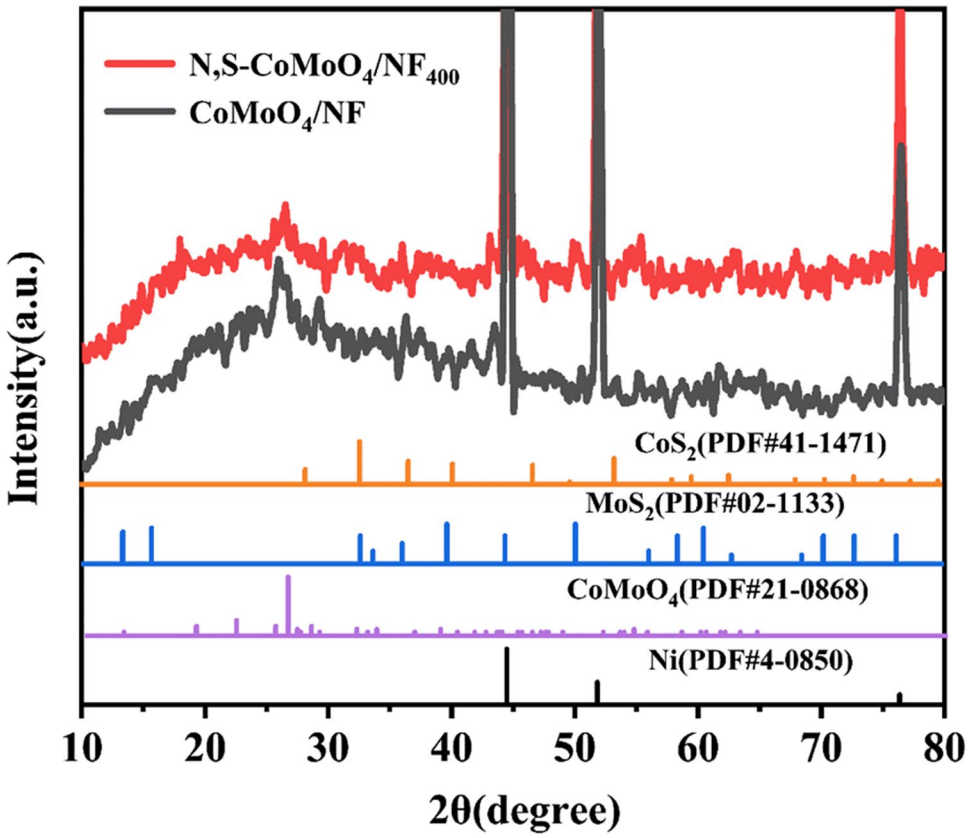

Fig. 3 XRD patterns of N, S-CoMoO4/NF400 and CoMoO4/NF

Transmission electron microscopy (TEM) was also performed to further reveal the microstructure and morphology of N, S-$CoMoO_4/NF_{400}$. Figure 4a and b are TEM images of the N, S-$CoMoO_4/NF_{400}$ nanosheet, which is agreeable to

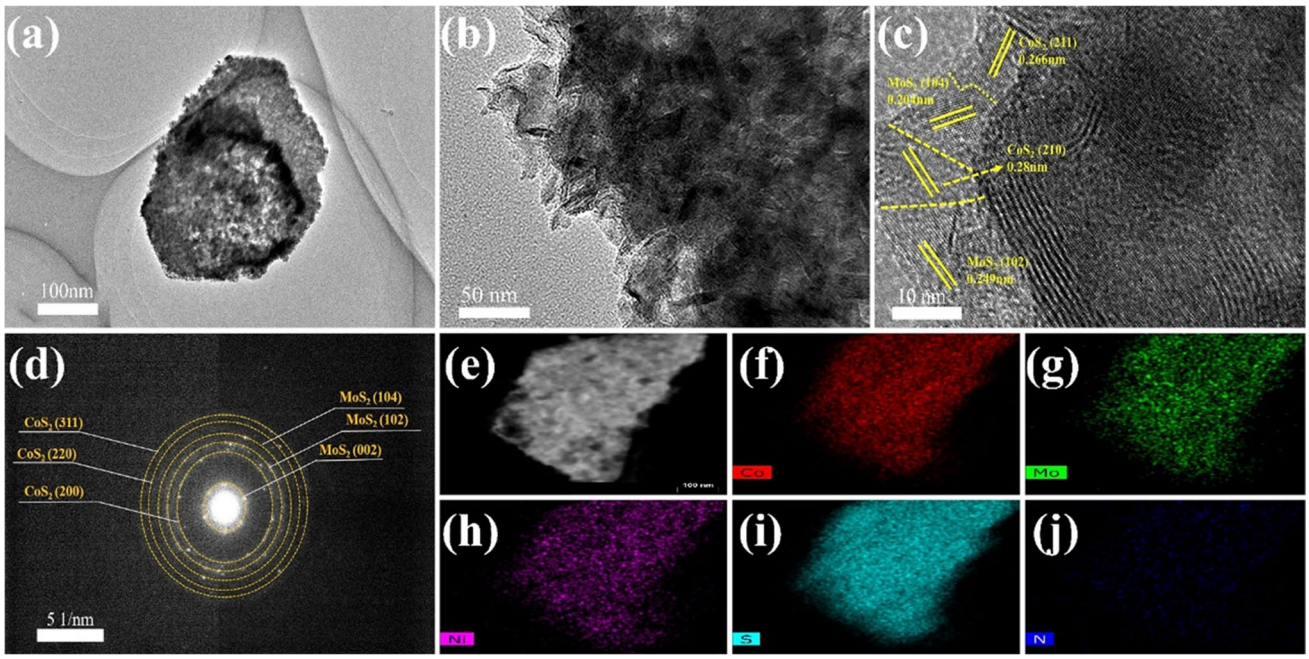

Fig. 4 (**a**–**b**) TEM and (**c**) HRTEM images of N, S-CoMoO4/NF400, (**d**) SAED pattern of N, SCoMoO4/NF, (**e**) Dark-field TEM (DFTEM) images and (**f**–**j**) corresponding elemental maps of N, S-CoMoO4/NF for Co, Mo, Ni, S, and N

the micromorphology observed in the SEM images. Close observation reveals that these ultra-thin nanosheets possess the rough and porous surface. This porous nanosheet structure possesses more active centers, which contributes to the transfer of electrons and optimizes the electrochemical performance of the catalyst. In Fig. 4c, the high-resolution TEM (HRTEM) image clearly displays the N, S-$CoMoO_4$ film grown on the nickel foam. And carefully observed, the N, S-$CoMoO_4$ film has the characteristics of MoS_2 layered structure. The HRTEM images exhibit lattice stripes with planar spacing of 0.217 and 0.336 nm, corresponding to the (222) and (002) planes of $CoMoO_4$. The crystalline surface of MoS_2 and CoS_2 can also be observed in the N, S-$CoMoO_4$ film. Remarkably, the mismatch between the lattices of CoS_2 and MoS_2 will produce numerous defects. The interface and defects promote fast electron transfer, which increases the catalytic activity. The SAED pattern shows multiple concentric circles, showing (222) and (002) planes of $CoMoO_4$, (200) planes of CoS_2, and (103) planes of MoS_2, which proves the N, S-$CoMoO_4$/NF_{400} polycrystalline properties (Fig. 4d). Figure 4e-j shows the DFTEM images of N, S-$CoMoO_4$/NF_{400} and the corresponding EDX elemental mapping images of Co, Mo, Ni, S and N. Additionally, Figure S6 demonstrates the contents of the five elements. The five elements are uniformly distributed in the entire nanosheet array, indicating the successful incorporation of N and S into the $CoMoO_4$ crystal, in agreement with the XRD results.

The chemical valence states of N, S-$CoMoO_4$/NF_{400} were analyzed by XPS analysis. The coexistence of Co, Mo, Ni, N, S, and O is evidenced by the XPS survey in Fig. 5a. For Mo 3d, the characteristic peak of Mo^{6+} binding energy of 235.8 eV indicates partial oxidation of Mo to MoO_3. Similarly, the peaks of Mo^{4+} $3d_{3/2}$ and $3d_{5/2}$ are 232.79 eV and 229.24 eV, and the peak of Mo-S bond is 226.9 eV (Fig. 5b) [36]. In comparison, the XPS spectra of the Co 2p region are rather weak, indicating that the relatively small amount of CoS_2 present in the nanocomposites (Fig. 5c), which is consistent with the EDX mapping analysis. The binding energy peaks at 797.1 eV and 779.2 eV correspond to Co^{3+} $2p^{1/2}$ and $2p^{3/2}$, and the peaks at 799.2 eV and 782.4 eV are assigned to Co^{2+} $2p^{1/2}$ and $2p^{3/2}$ [11]. The slightly higher binding energy of the Co^{2+} species is likely attributed to the strong electron-withdrawing effect of the coordinated N, which indicates the presence of Co – N catalytic active sites [37]. And the presence of Co^{3+} species is caused by the strong electronegativity of N and S, which changes the electronic structure of the Co nucleus, leads to an elevation of the valence state and facilitates the desorption of the active H atoms [38]. Figure 5d shows the high-resolution S 2p spectrum in N,S-$CoMoO_4$/NF_{400}, which is decomposed into two peaks along with a shaky satellite peak (SO_4^{2-})

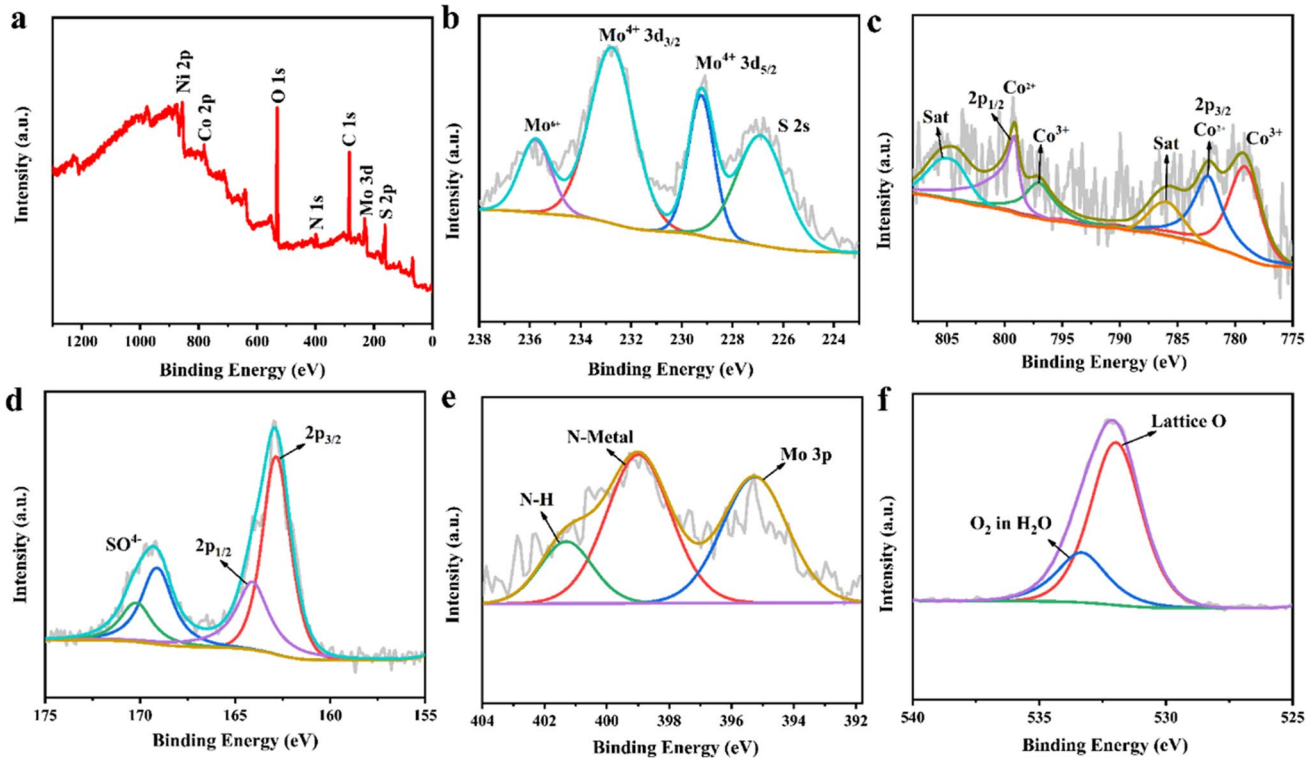

Fig. 5 High-resolution XPS spectra of (a) survey, (b) Co 2p, (c) Mo 3d, (d) S 2p, (e) N 1 s and (f) O 1 s for N, S-CoMoO4/NF400

[39]. The peaks at 164.1 and 162.9 eV are considered as S $2p_{1/2}$ and S $2p_{3/2}$ in N, S-$CoMoO_4$/NF_{400}. The spectrum of N 1 s (Fig. 5e) is characterized by the presence of three peaks located at 395.3, 398.9 and 401.3 eV. The peak at 401.3 eV corresponds to the N–H group, which is believed to facilitate the HER process [40]. The two peaks at 398.9 and 395.3 eV belong to the N-metal bond and Mo 3p, respectively. The above results demonstrate the successful incorporation of N and S elements. Figure 5f shows the O 1 s spectra which are associated with partial oxidation, and the obtained electrocatalyst peaks at 533.4 and 531.9 eV match the absorption of water molecules and lattice O (Co–O and Mo–O), respectively [17]. These results suggest that the co-doping strategy of nitrogen and sulfur could have a role in modulating the electronic structure of $CoMoO_4$. That is, after doping with nitrogen and sulfur, the electrons of $CoMoO_4$ are transferred to N and S atoms, resulting in a decrease in electron density. The co-doping of N, S atoms decreases the electron density of metal ions and O atoms which results in a reduction of the bond energy of metal-O bonds. This situation diminishes the hydrogen adsorption, promotes hydrogen release and accelerates the catalytic decomposition process [24]. The above discussion confirms the preparation of N, S-$CoMoO_4$/NF_{400}, which is consistent with all previous characterization results. Based on these analyses, N, S co-doping ultrathin nanosheet arrays are successfully constructed. The flower cluster-like structure formed by the stacked nanosheets can boost the rate of electron transition and accelerate the release of H_2. It will be beneficial to improve the HER performance of the electrocatalyst.

The above structural characterization demonstrates that ultrathin porous N, S-$CoMoO_4$/NF_{400} nanosheets are prepared on nickel foam substrates. The HER performance of the prepared electrocatalysts was evaluated in 1.0 M saturated KOH solution. In comparison with other samples, N, S-$CoMoO_4$/NF_{400} demonstrates excellent HER activity with an operating potential of 58 mV at a current density of 10 mA cm^{-2}, which is significantly outperformed N-$CoMoO_4$/NF (69 mV), S-$CoMoO_4$/NF (72 mV) and $CoMoO_4$/NF (283 mV) (Fig. 6a). The good catalytic performance certifies the essential role of the N, S co-doping for the boosted HER activity. Furthermore, comparing their overpotentials when operating at large current densities, N, S-$CoMoO_4$/NF_{400} can provide overpotentials of 102 and 119 mV at 50 and 100 mA cm^{-2} (Fig. 6b and Fig. 6c). It is noticeable that the overpotential of N, S-$CoMoO_4$/NF_{500} and N, S-$CoMoO_4$/NF_{400} at low current densities are approximately equal. However, the overpotential of N, S-$CoMoO_4$/NF_{500} increases significantly at large current densities. The XRD result reveals that the sample produces a NiS_2 phase at 500 °C, which improves the HER performance. The catalyst is excessively brittle due to annealing under high temperatures, so it is unable to operate stably at high currents. With the combination of the above results, the best HER performance of the ultrathin porous nanosheets prepared by co-doping $CoMoO_4$ with N and S at 400 °C can be demonstrated.

Accordingly, Tafel slopes of 48.68, 103.09, 61.49, 68.63, 73.23 and 81.29 mV dec^{-1} for N, S-$CoMoO_4$/NF_{400}, $CoMoO_4$/NF, N-$CoMoO_4$/NF, N, S-$CoMoO_4$/NF_{500}, S-$CoMoO_4$/NF and N, S-$CoMoO_4$/NF_{300} are obtained, respectively (Fig. 6d), indicating the excellent reaction kinetics of N, S-$CoMoO_4$/NF_{400}. Typically, there are two reactions involved in the HER process in alkaline solutions. The Volmer reaction is first performed, where water dissociates on the catalyst surface into adsorbed H atoms and OH^-. Then, the Tafel reaction or Heyrovsky reaction occurs, enabling the adsorbed H atoms to combine and produce H_2 [41]. The Tafel values reveal that the HER catalytic process of N, S-$CoMoO_4$/NF_{400} obeys the Volmer-Heyrovsky mechanism and the electrochemical desorption of hydrogen is the key step. For the materials composition, although each component has significance in the catalysts, the active site of HER is mainly dependent on the anionic active center, M-S, and M–N (M: Co, Mo) edge sites. N and S atoms replaced O atoms, and bonded with Co and Mo atoms to lead to a weakening of the free energy of adsorbed H and promote the desorption of H atoms [30, 42]. Furthermore, the N atom could replace the S sites in M-S [43]. In comparison to S atoms, N is more electronegative and changes the electron density of metal atoms more, which facilitates the HER process. For the structure, it is clear from the TEM images that the catalysts possess an abundance of interfaces, which accelerates the electron transfer rate. The structural advantages of the catalysts and more anionic active centers improve the electrochemical reaction kinetics. In summary, simultaneous doping of N, S elements in the catalysts can make N, S-$CoMoO_4$/NF_{400} possibly easier to break H–O-H bonds and increase adsorbed H, resulting in beneficial HER catalytic activity compare to $CoMoO_4$/NF, S-$CoMoO_4$/NF and N-$CoMoO_4$/NF [17, 44]. Similarly, the experimental results reveal that the Tafel slope of N, S-$CoMoO_4$/NF_{400} decreased from 103.09 to 48.68 mV dec^{-1}, indicating that the hydrolysis kinetics of the Volmer reaction was accelerated during the doping process.

Cyclic voltammetry measurements were obtained for the double layer capacitance and estimated electrochemically active surface area (ECSA). Figure S7 presents the CV curves of all prepared catalysts at scan rates from 5 to 25 mV s^{-1}. As shown in Fig. 6e, N,S-$CoMoO_4$/NF_{400} displays the optimum Cdl value (125.81 mF cm^{-2}), which is in preference to N-$CoMoO_4$/NF (88.48 mF cm^{-2}), S-$CoMoO_4$/NF (67.72 mF cm^{-2}), N, S-$CoMoO_4$/NF_{500} (47.32 mF cm^{-2}), N, S-$CoMoO_4$/NF_{300} (20.3 mF cm^{-2}) and $CoMoO_4$/NF (2.6 mF cm^{-2}), suggesting that the $CoMoO_4$ nanosheet arrays co-doped with N and S elements expose more active sites.

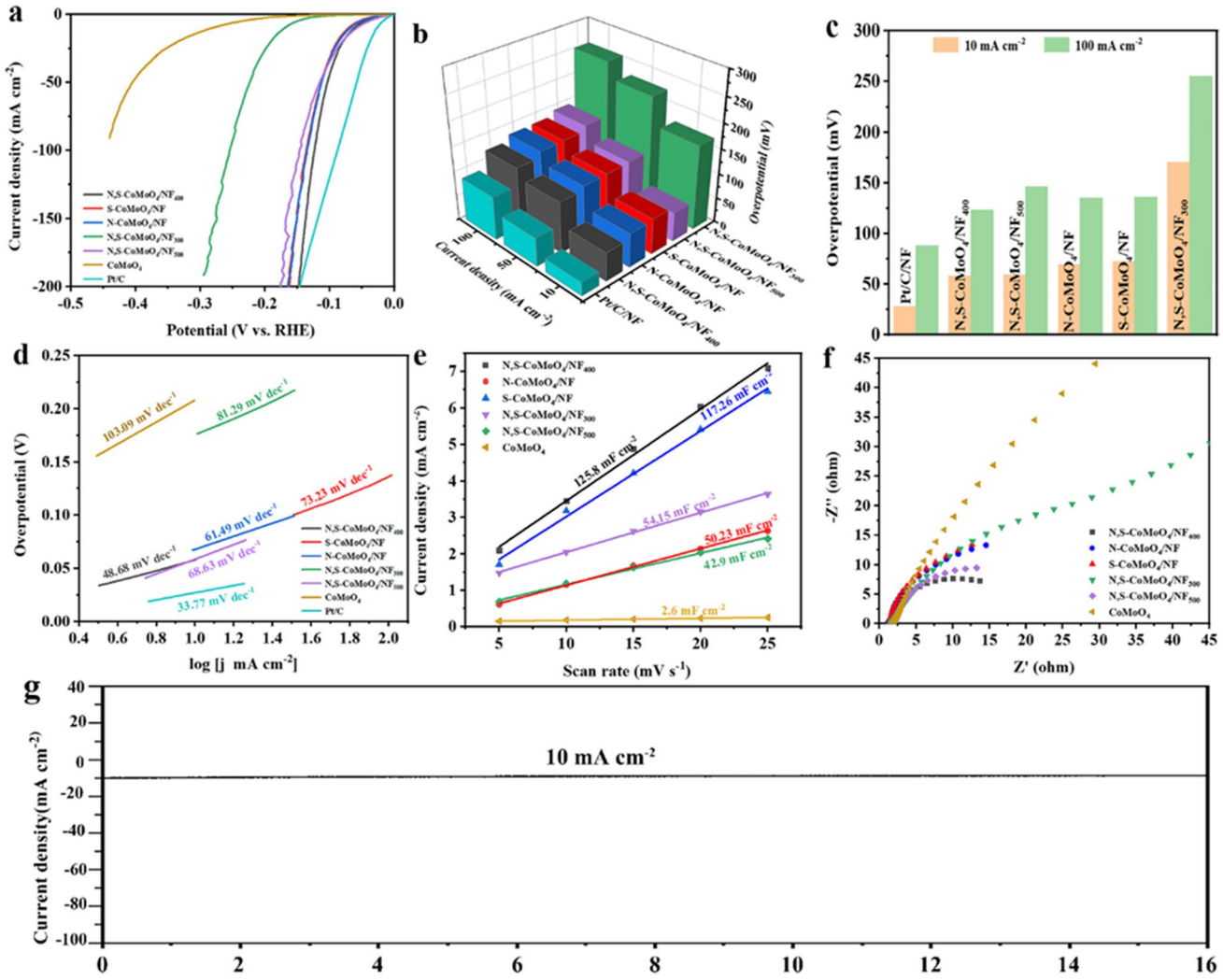

Fig. 6 HER performance of different catalysts: (a) polarization curves, (b)–(c) comparison of the overpotential at the current densities of 10, 50 and 100 mA cm^{-2}, (d) Tafel plots of different electrodes, (e) Capacitive current versus scan rate, (f) Nyquist plot of the prepared catalyst, (g) polarization curves before and after 1000 cycles for N, S-NCO@CMO_{400}, (h) chronoamperometry curve at 10 mA cm^{-2} and (i) chronoamperometry curve at 200 mA $cm.^{-2}$

Further EIS studies were used to reveal the effect of N and S atoms on the HER process of the electrocatalyst. The N, S-$CoMoO_4/NF_{400}$ electrode shows a smaller charge transfer resistance (Rct) compared to $CoMoO_4$/NF, S-$CoMoO_4$/NF_{400}, N-$CoMoO_4/NF_{400}$, N, S-$CoMoO_4/NF_{300}$ and N, S-$CoMoO_4/NF_{500}$ (Fig. 6f). It indicates that the interfacial electron transfer rate was accelerated after co-doping with N and S, which improves the HER performance. The agreement of ESCA, EIS, Tafel and LSV results proves the best electrochemical activity of the N, S-$CoMoO_4/NF_{400}$ electrode. The above results are in accordance with the expected findings of SEM, XRD, TEM and demonstrate that the nanosheet arrays have a great enhancement effect on the HER performance of N, S-$CoMoO_4/NF_{400}$. It is further shown that N, S co-doping could effectively modulate the electronic structure and surface chemistry of the catalyst, thus enhancing the catalytic activity of HER. As shown in Fig. 6g, the increment of cathodic potential was negligible after 1000 cycles. Figure 6h shows that the potential of N, S-$CoMoO_4/NF_{400}$ remains almost unchanged at 10 mA cm^{-2} for 16 h with a retention rate of 97.2%. Furthermore, the stability of N, S-$CoMoO_4/NF_{400}$ was measured at high current densities. The potential retention of the catalyst is 87.5% over 40 h when the current density is 200 mA cm^{-2} (Fig. 6i). It indicates that the HER of N, S-$CoMoO_4/NF_{400}$ nanosheet arrays on NF exhibits excellent stability in alkaline media. Moreover, it can be observed that the electrocatalytic activity of N,S-$CoMoO_4/NF_{400}$ for HER is significantly superior to those reported high-performance of hydrogen evolution electrocatalysts [35, 44–62], such as N-Co-S/G (67.7 mV) [35],

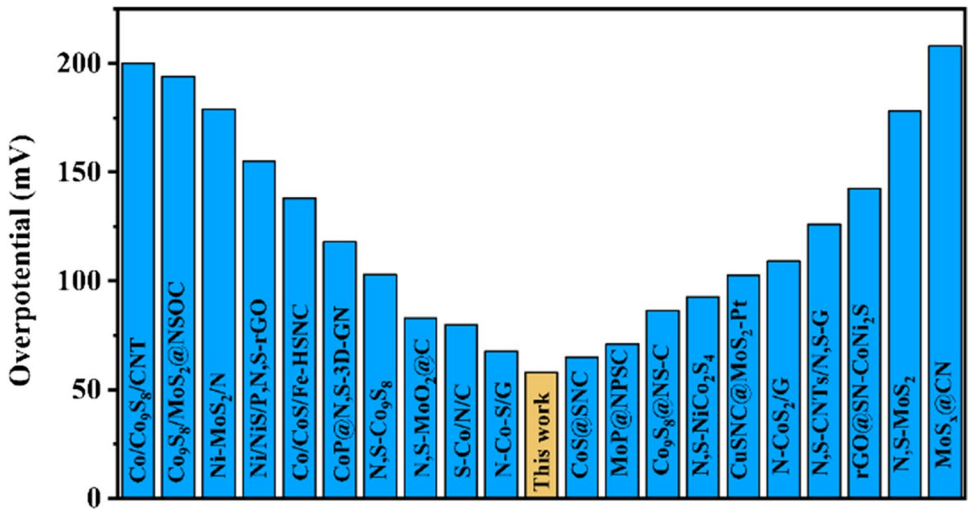

Fig. 7 Comparison of the overpotential at 10 mA cm^{-2} during HER in the present work with the reported electrocatalysts

CuSNC@MoS_2-Pt(102.6 mV) [44], N,S-$NiCo_2S_4$ (92.7 mV) [45], N,S-CNTs/N,S-G (126 mV) [46], CoP@N,S-3D-GN (118 mV) [47], N,S-Co_9S_8 (103 mV) [48], N,S co-doped MoO_2@C (83 mV) [49], and so on (Fig. 7).

Conclusion

In summary, we report the synthesis of an exquisitely designed nanosheet array of N, S-$CoMoO_4$/NF_{400} electrocatalysts with ultrathin porous structures. The surface properties are modified by direct doping with N and S elements to improve the HER performance of the electrocatalyst. With the advantage of its structure and composition, N, S-$CoMoO_4$/NF_{400} exhibits excellent HER property with overpotential of 58,119 mV at current densities of 10 and 100 mA cm^{-2}. In addition, N, S-$CoMoO_4$/NF_{400} can operate stably for 16 h at a current density of 10 mA cm^{-2}. Based on the above findings, this study facilitates the exploration of electrocatalysts with great catalytic activity for hydrogen evolution reaction.

Supplementary Information The online version contains supplementary material available at https://doi.org/10.1007/s11581-022-04707-z.

References

1. S Xu, S Gong, H Jiang, P Shi, J Fan, Q Xu, Y Min (2020) Z-scheme heterojunction through interface engineering for broad spectrum photocatalytic water splitting Applied Catalysis B: Environmental 267
2. Xia K, Guo J, Xuan C, Huang T, Deng Z, Chen L, Wang D (2019) Ultrafine molybdenum carbide nanoparticles supported on nitrogen doped carbon nanosheets for hydrogen evolution reaction. Chin Chem Lett 30:192–196
3. Q Che, Q Li, X Chen, Y Tan, X Xu (2020) Assembling amorphous (Fe-Ni)Co-OH/Ni_3S_2 nanohybrids with S-vacancy and interfacial effects as an ultra-highly efficient electrocatalyst: inner investigation of mechanism for alkaline water-to-hydrogen/oxygen conversion, Applied Catalysis B: Environmental 263
4. Jiang D, Ma W, Zhou Y, Xing Y, Quan B, Li D (2019) Coupling Co_2P and CoP nanoparticles with copper ions incorporated Co9S8 nanowire arrays for synergistically boosting hydrogen evolution reaction electrocatalysis. J Colloid Interface Sci 550:10–16
5. Liu Y, Li X, Zhang Q, Li W, Xie Y, Liu H, Shang L, Liu Z, Chen Z, Gu L, Tang Z, Zhang T, Lu S (2020) A general route to prepare low-ruthenium-content bimetallic electrocatalysts for pH-universal hydrogen evolution reaction by using carbon quantum dots. Angew Chem Int Ed Engl 59:1718–1726
6. Hatami E, Toghraei A, BaratiDarband G (2021) Electrodeposition of Ni–Fe micro/nano urchin-like structure as an efficient electrocatalyst for overall water splitting. Int J Hydrog Energy 46:9394–9405
7. Xu Y, Jiang X, Shao G, Xiang H, Si S, Li X, Hu TS, Hong G, Dong S, Li H, Feng Y, Liu S (2020) Interface effect of Ru-MoS_2 nanoflowers on lignin substrate for enhanced hydrogen evolution activity. Energy & Environmental Materials 4:117–125
8. Sun H, Yan Z, Liu F, Xu W, Cheng F, Chen J (2020) Self-supported transition-metal-based electrocatalysts for hydrogen and oxygen evolution. Adv Mater 32:e1806326
9. Wang Z, Chen J, Song E, Wang N, Dong J, Zhang X, Ajayan PM, Yao W, Wang C, Liu J, Shen J, Ye M (2021) Manipulation on active electronic states of metastable phase beta-NiMoO4 for large current density hydrogen evolution. Nat Commun 12:5960
10. He W, Cheng J, Gao Y, Liu C, Zhao J, Li Y, Hao Q (2021) Engineering sulfur vacancies into Fe9S10 nanosheet arrays for efficient alkaline hydrogen evolution. Nanoscale 13:12951–12955
11. Y Lu, X Guo, L Yang, W Yang, W Sun, Y Tuo, Y Zhou, S Wang, Y Pan, W Yan, D Sun, Y Liu (2020) Highly efficient CoMoS heterostructure derived from vertically anchored Co_5Mo_{10} polyoxometalate for electrocatalytic overall water splitting, Chemical Engineering Journal 394
12. Y Xu, R Wang, Y Zheng, L Zhang, T Jiao, Q Peng, Z Liu (2020) Facile preparation of self-assembled Ni/Co phosphates composite spheres with highly efficient HER electrocatalytic performances Applied Surface Science 509
13. Chen A, Fu L, Xiang W, Wei W, Liu D, Liu C (2021) Facile synthesis of Ni_5P_4 nanosheets/nanoparticles for highly active and durable hydrogen evolution. Int J Hydrogen Energy 46:11701–11710

14. Yan Q, Yang X, Wei T, Wu W, Yan P, Zeng L, Zhu R, Cheng K, Ye K, Zhu K, Yan J, Cao D, Wang G (2019) Self-supported cobalt–molybdenum oxide nanosheet clusters as efficient electrocatalysts for hydrogen evolution reaction. Int J Hydrogen Energy 44:21220–21228
15. Zhang T, Wu M-Y, Yan D-Y, Mao J, Liu H, Hu W-B, Du X-W, Ling T, Qiao S-Z (2018) Engineering oxygen vacancy on NiO nanorod arrays for alkaline hydrogen evolution. Nano Energy 43:103–109
16. M Wang, W Fu, L Du, Y Wei, P Rao, L Wei, X Zhao, Y Wang, S Sun (2020) Surface engineering by doping manganese into cobalt phosphide towards highly efficient bifunctional HER and OER electrocatalysis Applied Surface Science 515
17. Xie W, Yu T, Ou Z, Zhang J, Li R, Song S, Wang Y (2020) Self-Supporting clusters constituted of nitrogen-doped $CoMoO_4$ nanosheets for efficiently catalyzing the hydrogen evolution reaction in alkaline media. ACS Sustain Chem Eng 8:9070–9078
18. Bau JA, Kozlov SM, Azofra LM, Ould-Chikh S, Emwas A-H, Idriss H, Cavallo L, Takanabe K (2020) Role of oxidized Mo species on the active surface of Ni–Mo electrocatalysts for hydrogen evolution under alkaline conditions. ACS Catal 10:12858–12866
19. Zhang L, Cao X, Feng C, Zhang W, Wang Z, Feng S, Huang Z, Lu X, Dai F (2021) Interfacial Mo-N-C bond endowed hydrogen evolution reaction on MoSe2@N-doped carbon hollow nanoflowers. Inorg Chem 60:12377–12385
20. C Huang, D Wu, P Qin, K Ding, C Pi, Q Ruan, H Song, B Gao, H Chen, PK Chu (2020) Ultrafine Co nanodots embedded in N-doped carbon nanotubes grafted on hexagonal VN for highly efficient overall water splitting, Nano Energy 73
21. Ma X, Wei B, Yuan M, Li J, Liang S, Wu Y, Dai D, Xu L (2020) Self-supported phosphorus-doped $CoMoO_4$ rod bundles for efficient hydrogen evolution. J Mater Sci 55:6502–6512
22. Chai L, Hu Z, Wang X, Xu Y, Zhang L, Li TT, Hu Y, Qian J, Huang S (2020) Stringing bimetallic metal-organic framework-derived cobalt phosphide composite for high-efficiency overall water splitting. Adv Sci (Weinh) 7:1903195
23. Chen WF, Muckerman JT, Fujita E (2013) Recent developments in transition metal carbides and nitrides as hydrogen evolution electrocatalysts. Chem Commun (Camb) 49:8896–8909
24. C Huang, L Yu, W Zhang, Q Xiao, J Zhou, Y Zhang, P An, J Zhang, Y Yu (2020) N-doped Ni-Mo based sulfides for high-efficiency and stable hydrogen evolution reaction Applied Catalysis B: Environmental 276
25. Fan W, Wang D, Sun Z, Ling XY, Liu T (2019) Graphene/graphene nanoribbon aerogels decorated with S-doped MoSe2 nanosheets as an efficient electrocatalyst for hydrogen evolution, Inorganic Chemistry. Frontiers 6:1209–1216
26. T Sun, P Liu, Y Zhang, Z Chen, C Zhang, X Guo, C Ma, Y Gao, S Zhang (2020) Boosting the electrochemical water splitting on Co_3O_4 through surface decoration of epitaxial S-doped CoO layers Chemical Engineering Journal 390
27. Wang J, Tran DT, Chang K, Prabhakaran S, Kim DH, Kim NH, Lee JH (2021) Bifunctional catalyst derived from sulfur-doped $VMoO_x$ nanolayer shelled Co nanosheets for efficient water splitting. ACS Appl Mater Interfaces 13:42944–42956
28. Naveen MH, Huang Y, BisalereKantharajappa S, Seo K-D, Park D-S, Shim Y-B (2020) Enhanced electrocatalytic activities of in situ produced Pd/S/N-doped carbon in oxygen reduction and hydrogen evolution reactions. ACS App Energy Mater 4:575–585
29. Gong Y, Wang L, Xiong H, Shao M, Xu L, Xie A, Zhuang S, Tang Y, Yang X, Chen Y, Wan P (2019) 3D self-supported Ni nanoparticle@N-doped carbon nanotubes anchored on NiMoN pillars for the hydrogen evolution reaction with high activity and anti-oxidation ability. Journal of Materials Chemistry A 7:13671–13678
30. J Sun, W Xu, C Lv, L Zhang, M Shakouri, Y Peng, Q Wang, X Yang, D Yuan, M Huang, Y Hu, D Yang, L Zhang (2021) Co/MoN hetero-interface nanoflake array with enhanced water dissociation capability achieves the Pt-like hydrogen evolution catalytic performance. Applied Catalysis B: Environmental 286
31. K Ji, K Matras-Postolek, R Shi, L Chen, Q Che, J Wang, Y Yue, P Yang (2022) MoS_2/CoS_2 heterostructures embedded in N-doped carbon nanosheets towards enhanced hydrogen evolution reaction. Journal of Alloys and Compounds 891
32. Tian XL, Wang L, Chi B, Xu Y, Zaman S, Qi K, Liu H, Liao S, Xia BY (2018) Formation of a tubular assembly by ultrathin $Ti_{0.8}Co_{0.2}N$ nanosheets as efficient oxygen reduction electrocatalysts for hydrogen–/metal–air fuel cells. ACS Catalysis 8:8970–8975
33. Jaramillo TF, Bonde J, Zhang J, Ooi B-L, Andersson K, Ulstrup J, Chorkendorff I (2008) Hydrogen evolution on supported incomplete cubane-type $[Mo_3S_4]^{4+}$ electrocatalysts. J Phys Chem C 112:17492–17498
34. J Li, H Huang, X Cao, H-H Wu, K Pan, Q Zhang, N Wu, X Liu (2021) Template-free fabrication of MoP nanoparticles encapsulated in N-doped hollow carbon spheres for efficient alkaline hydrogen evolution. Chem Eng J 416
35. P Sabhapathy, I Shown, A Sabbah, P Raghunath, J-L Chen, W-F Chen, M-C Lin, K-H Chen, L-C Chen (2021) Electronic structure modulation of isolated Co-N_4 electrocatalyst by sulfur for improved pH-universal hydrogen evolution reaction. Nano Energy 80
36. J Yang, C Zhang, Y Niu, J Huang, X Qian, K-Y Wong (2021) N-doped C-CoS_2@CoS_2/MoS_2 nano polyhedrons with hierarchical yolk-shelled structures as bifunctional catalysts for enhanced photovoltaics and hydrogen evolution. Chem Eng J 409
37. Deng C, Wu KH, Scott J, Zhu S, Zheng X, Amal R, Wang DW (2019) Spherical Murray-type assembly of Co-N-C nanoparticles as a high-performance trifunctional electrocatalyst. ACS Appl Mater Interfaces 11:9925–9933
38. L Zhu, L Liu, G Huang, Q Zhao (2020) Hydrogen evolution over N-doped CoS_2 nanosheets enhanced by superaerophobicity and electronic modulation Appl Surf Sci 504
39. M Kim, H Seok, N Clament Sagaya Selvam, J Cho, GH Choi, MG Nam, S Kang, T Kim, PJ Yoo (2021) Kirkendall effect induced bifunctional hybrid electrocatalyst (Co9S8@MoS2/N-doped hollow carbon) for high performance overall water splitting. J Power Sources 493
40. Gao W, Gou W, Zhou X, Ho JC, Ma Y, Qu Y (2018) Amine-modulated/engineered interfaces of NiMo electrocatalysts for improved hydrogen evolution reaction in alkaline solutions. ACS Appl Mater Interfaces 10:1728–1733
41. Y Lu, Z Li, Y Xu, L Tang, S Xu, D Li, J Zhu, D Jiang (2021) Bimetallic Co-Mo nitride nanosheet arrays as high-performance bifunctional electrocatalysts for overall water splitting. Chem Eng J 411
42. H Yu, W Zhang, S Miao, Y Du, Y Huang, D Tang, Z-A Qiao, J Wang, Z Zhao (2020) Synthesis of Co_9S_8 nanoparticle embedded, N, S Co-doped mesoporous carbon with salts as templates for electrocatalytic hydrogen evolution. Microporous Mesoporous Mater 302
43. Yu H, Miao S, Tang D, Zhang W, Huang Y, Qiao ZA, Wang J, Zhao Z (2020) A solvent-free strategy for synthesis of Co9S8 nanoparticles entrapped, N, S-codoped mesoporous carbon as hydrogen evolution electrocatalyst. J Colloid Interface Sci 558:155–162
44. J Rong, G Zhu, W Ryan Osterloh, Y Fang, Z Ou, F Qiu, KM (2021) Kadish, In situ construction MoS2-Pt nanosheets on 3D MOF-derived S, N-doped carbon substrate for highly efficient alkaline hydrogen evolution reaction. Chem Eng J 412
45. H Li, L Chen, P Jin, Y Li, J Pang, J Hou, S Peng, G Wang, Y Shi (2021) $NiCo_2S_4$ microspheres grown on N, S co-doped reduced

graphene oxide as an efficient bifunctional electrocatalyst for overall water splitting in alkaline and neutral ph. Nano Res
46. W. Zhao, B. Hu, B. Xiong, J. Ye, Q. Yang, P. Fan, M. Nie, Y. Jin, L. Fang, W.Q. Tian, Temperature differentiated synthesis of hierarchically structured N,S-Doped carbon nanotubes/graphene hybrids as efficient electrocatalyst for hydrogen evolution reaction, Journal of Alloys and Compounds, 848 (2020).
47. C. Karaman, O. Karaman, N. Atar, M.L. Yola, Tailoring of cobalt phosphide anchored nitrogen and sulfur co-doped three dimensional graphene hybrid: boosted electrocatalytic performance towards hydrogen evolution reaction, Electrochimica Acta, 380 (2021).
48. Yu H, Sun X, Tang D, Huang Y, Zhang W, Miao S, Qiao Z-A, Wang J, Zhao Z (2020) Molten salt strategy to synthesize alkali metal-doped Co_9S_8 nanoparticles embedded, N, S co-doped mesoporous carbon as hydrogen evolution electrocatalyst. Int J Hydrogen Energy 45:6006–6014
49. B.A. Yusuf, M. Xie, N. Ullah, C.J. Oluigbo, W. Yaseen, J. Xie, Y. Xu, Facile synthesis of N, S co-doped MoO_2@C nanorods as an outstanding electrocatalyst for hydrogen evolution reaction, Applied Surface Science, 537 (2021).
50. B-L Deng, L-P Guo, Y Lu, H-B Rong, D-C Cheng (2021) Sulfur–nitrogen co-doped graphene supported cobalt–nickel sulfide rGO@SN-CoNi2S4 as highly efficient bifunctional catalysts for hydrogen/oxygen evolution reactions. Rare Metals
51. Bereketova A, Nallal M, Yusuf M, Jang S, Selvam K, Park KH (2021) A Co-MOF-derived flower-like CoS@S, N-doped carbon matrix for highly efficient overall water splitting, RSC. Advances 11:16823–16833
52. Tong Y, Sun Q, Chen P, Chen L, Fei Z, Dyson PJ (2020) Nitrogen-incorporated cobalt sulfide/graphene hybrid catalysts for overall water splitting. Chemsuschem 13:5112–5118
53. Hegazy MBZ, Berber MR, Yamauchi Y, Pakdel A, Cao R, Apfel UP (2021) Synergistic electrocatalytic hydrogen evolution in Ni/NiS nanoparticles wrapped in multi-heteroatom-doped reduced graphene oxide nanosheets. ACS Appl Mater Interfaces 13:34043–34052
54. Juan P, Liang J, Chen T, Zhang Q, Peng W, Li Y, Zhang F, Fan X (2020) Sulfur-rich molybdenum sulfide grown on porous N-Doped graphene for efficient hydrogen evolution. Ind Eng Chem Res 59:12862–12869
55. Zhang H-M, Zhu C (2020) Co nanoparticles-embedded N S-codoped hierarchically porous graphene sheets as efficient bifunctional electrocatalysts for oxygen reduction reaction and hydrogen evolution reaction. J Mater Res Technol 9:16270–16279
56. X Zhang, Y Wang, K Wang, Y Huang, D Lyu, F Yu, S Wang, ZQ Tian, PK Shen, SP Jiang (2021) Active sites engineering via tuning configuration between graphitic-N and thiophenic-S dopants in one-step synthesized graphene nanosheets for efficient water-cycled electrocatalysis. Chem Eng J 416
57. B Liu, Y Cheng, B Cao, M Hu, P Jing, R Gao, Y Du, J Zhang, J Liu (2021) Hybrid heterojunction of molybdenum disulfide/single cobalt atoms anchored nitrogen, sulfur-doped carbon nanotube/cobalt disulfide with multiple active sites for highly efficient hydrogen evolution Appl Catalysis B: Environ 298
58. Y Liu, X Luo, C Zhou, S Du, D Zhen, B Chen, J Li, Q Wu, Y Iru, D Chen (2020) A modulated electronic state strategy designed to integrate active HER and OER components as hybrid heterostructures for efficient overall water splitting. Appl Catalysis B: Environ 260
59. A Ashok, A Kumar, J Ponraj, SA Mansour (2021) Development of Co/Co_9S_8 metallic nanowire anchored on N-doped CNTs through the pyrolysis of melamine for overall water splitting. Electrochimica Acta 368
60. T Dong, X Zhang, P Wang, H-S Chen, P Yang (2020) Formation of Ni-doped MoS_2 nanosheets on N-doped carbon nanotubes towards superior hydrogen evolution. Electrochimica Acta 338
61. Li Y-W, Wu Q, Ma R-C, Sun X-Q, Li D-D, Du H-M, Ma H-Y, Li D-C, Wang S-N, Dou J-M (2021) A Co-MOF-derived Co_9S_8@NS-C electrocatalyst for efficient hydrogen evolution reaction. RSC Adv 11:5947–5957
62. Chen T-T, Wang R, Li L-K, Li Z-J, Zang S-Q (2020) MOF-derived Co_9S_8/MoS_2 embedded in tri-doped carbon hybrids for efficient electrocatalytic hydrogen evolution, Journal of Energy. Chemistry 44:90–96